Isothermal Pyrolysis of Low-Rank Coal: Kinetic Study, Batch Experiments, and Product Analysis

Abstract

Effective use of low-grade coal is essential for meeting worldwide energy needs and minimizing ecological effects, which makes studying its thermal decomposition a key focus for sustainable energy development. Understanding the pyrolytic degradation process of coal is crucial for optimizing its use in eco-friendly energy solutions. It is hypothesized that the isothermal pyrolysis of low-rank coal at different temperatures will exhibit different kinetic behaviors and produce valuable condensable products. This research investigates the pyrolytic behavior, kinetics, and batch pyrolysis of low-rank coal. Thermo-gravimetric analysis was conducted under isothermal conditions at temperatures ranging from 350 to 500 °C, with a 25 °C increment, for 2 hours in an inert atmosphere. The data were analyzed using model-fitting methods, testing a total of 21 models to calculate the reaction kinetics. The results revealed that weight loss increased with temperature, reaching a maximum at 18.61% (450 °C), with activation energies of 5.817–123.51 kJ/mol. The D2 diffusion model best described the process (Ea = 7.267 kJ/mol, A = 0.022 min^{-1}). The pyrolysis index rose from 0.0113 (350 °C) to 0.051 (500 °C). At 450°C, 18.9% condensable products formed, containing alkanes, alicyclics, and aromatics (FTIR/GC-MS). These findings aid in optimizing sustainable pyrolysis of low-rank coal for valuable outputs.

Keywords: Batch pyrolysis, Isothermal pyrolysis, low-rank coal, Model-fitting, Pyrolysis index

1. Introduction

Compared to other fossil fuels, coal is more affordable, available, and plentiful. Many nations, including India, the United States, China, and Australia, have seen a financial boom as a result of the presence of coal reserves [1]. In 2022–23, India produced 893.190 MT of raw coal, marking a 14.77% increase from 778.210 MT in 2021–22. Odisha led coal production in 2022–23 with 218.981 MT, followed by Chhattisgarh (184.895 MT), Jharkhand (156.445 MT), and Madhya Pradesh (146.028 MT) [2]. India gets 55 % of its energy from coal [3]. Additionally, coal is used in the sponge iron industry, cement industry, fertilizers industry, chemicals industry, steel industry, etc. [4]. Thus, the marketable main energy utilization of India has increased by more than 700 % during the previous 40 years [5]. India has large deposits of low-grade coal [6]. Lignite, a low-grade coal with minimal carbon content [7]. Lignite production in India during 2022–23 was 44.990 MT, a 5.27% decrease from 47.492 MT in 2021–22. Lignite deposits in India are mainly found in the Tertiary sediments of the Southern and Western peninsular shield, particularly in Tamil Nadu, Pondicherry, Gujarat, Rajasthan, and Jammu & Kashmir, with smaller quantities in Odisha, Kerala, and West Bengal. The top lignite producers during 2022–23 were Tamil Nadu with 22.480 MT, Gujarat with 12.313 MT, and Rajasthan with 10.197 MT [2]. Direct use of these coals for energy generation is unsuitable because of their poor energy yield and harmful environmental and health impacts. Therefore, developing sustainable and eco-friendly coal conversion methods is essential to address growing energy needs. Pyrolysis of such coal could produce high-energy-density liquid and gaseous fuel along with coke [6]. Successful transformation of low-rank coal into high-energy fuels necessitates a complete understanding of its thermal decomposition characteristics and reaction kinetics.

Several studies on the non-isothermal kinetics of coal have been reported, summarised below. Dwivedi et al. pyrolyzed three samples of Indian coal in the range of 30-950 °C temperature and 50, 100, 150, and 200 K/min heating rates, in a nitrogen atmosphere. The activation energy (Ea) value of Indian coal determined by the Friedman Method is 49.132 kJ/mol [6]. Research by Sabat et al. examined the thermal decomposition kinetics of three coal grades (10, 13, and 14) under varying heating rates, employing first-order reaction models to determine average activation energies. The activation energy values calculated for Grade-10, Grade-13, and Grade-14 coal are 62.114, 61.940, and 57.563 kJ/mol, respectively [8]. Dong et al. performed the pyrolysis of various Indian coals at heating rates changing from 278 to 773 K/min and reported that the activation energy of Indian coals ranged from 428.78 to 520 kJ/mol, computed by using the Friedman method [9]. Prabhakar et al. pyrolyze the coal fines under non-isothermal conditions in a nitrogen atmosphere at 20, 30, and 40 °C/min heating rates and reported the activation energy (Ea) (31.41 kJ/mol to 50.42 kJ/mol) and Arrhenius factor (A) value (1.05×10^{6} to 1.4×10^{7} min^{-1}) calculated by using the isoconversional method [10]. Research by Yan et al. demonstrated that thermal decomposition progressively converts aliphatic carbon into aromatic structures in subbituminous coals, with both cluster size and molecular weight growing with coal rank. Concurrently, the activation energy distribution narrowed as rank increased [11]. Casa et al. reported that among different coal types, lignite showed the lowest pyrolysis activation energy (73 kJ/mol), whereas anthracite exhibited the highest (138 kJ/mol). Bituminous coal displayed intermediate values between 97-117 kJ/mol [12]. According to Guo et al., increasing the heating rate causes an increase in both the initial and final reaction temperatures and has a significant impact on coal pyrolysis. The highest Ea is found in the 850-930 °C temperature range. The lowest activation energy is seen at a 15 °C/min heating rate. Greater hydrogen production occurs when coal is heated at 15 °C/min heating rate in a fixed-bed reactor [13]. Ashraf et al. investigated the thermal degradation behavior of CC and DC coals under non-isothermal conditions, applying heating rates ranging from 10-40 °C/min (in 10 °C intervals).The average Ea values for CC and DC were calculated using the Friedman differential isoconversional model, yielding values of 134.54 and 129.81 kJ/mol, respectively [14]. Gao et al. observed that both activation energy (Ea) and pre-exponential factor (A) rose proportionally with heating rate during coking coal pyrolysis. Their study found these parameters remained unaffected by particle size variations, and noted that coking coal consistently demonstrated higher Ea values compared to non-coking varieties [15].

While non-isothermal techniques have dominated solid-state kinetic analysis for decades, isothermal methods are increasingly preferred due to their practical advantages. Unlike dynamic heating approaches, isothermal analysis simplifies kinetic parameter determination by eliminating temperature gradients and non-stationary heat transfer effects. By maintaining constant temperature conditions, this method allows more straightforward identification of reaction mechanisms and orders, as it avoids the complexities introduced by varying heating rates in non-isothermal experiments [16]. A few reports on the isothermal kinetic analysis of coal reported in the literature are summarised as follows.

Jeong et al. investigated the pyrolysis of coking coal blended with biomass using both non-isothermal and isothermal methods in a thermogravimetric analyzer. For non-isothermal

pyrolysis, heating rates of 5, 10, 15, and 20 °C/min were applied from 25 °C to 800 °C, while isothermal pyrolysis was performed between 500–800 °C. The study found that weak coking coal (WCC) exhibited higher activation energy (252.08–579.4 kJ/mol) compared to hard coking coal (HCC) (163.7–272.45 kJ/mol) under non-isothermal conditions. Additionally, HCC/biomass blends had lower activation energies (88.71–400.98 kJ/mol) than WCC/biomass blends (127.7–456.44 kJ/mol). Increasing the biomass proportion in the blends reduced activation energy for both coal types. Under isothermal conditions, the activation energies for WCC and HCC blended with biomass were 42 kJ/mol and 40 kJ/mol, respectively [17]. Zhang et al. studied the pyrolysis kinetics of coal and oil shale under isothermal and non-isothermal conditions using a micro fluidized bed analyzer. Their findings revealed that the kinetic parameters, including activation energy (Ea) and pre-exponential factor (A), differed significantly between gas components. Notably, oil shale exhibited higher Ea and A values compared to both coal types[18]. Maria et al. examined the pyrolysis behavior of two Spanish coals (Mequinenza and Samca) under both isothermal (400, 500, and 600 °C) and non-isothermal conditions (heating rates of 5, 15, and 30 °C/min). Their results showed that isothermal runs had notably lower correlation coefficients compared to non-isothermal experiments. During non-isothermal pyrolysis, the mean activation energies for H_2 S and CO_2 were lower than those for CH_4 and CO in both coals, though this trend did not hold under isothermal conditions. The study also found that activation energies varied based on coal type, pyrolysis conditions (isothermal vs. non-isothermal), and temperature [19].

The literature review reveals a gap in the detailed isothermal kinetic studies of low-rank coal, particularly those incorporating batch pyrolysis and product characterization. In our earlier research, first-order model fitting was employed to thoroughly investigate the non-isothermal pyrolytic degradation behavior, kinetics, and thermodynamics of low-rank Indian coal across varying grades and heating rates [8, 20]. It was confirmed that grade 10 coal is the most optimal, with the primary non-isothermal thermal degradation zone occurring between 350-500 °C. Most studies in the literature typically use heating rates ranging from 1–20 °C/min for kinetic analysis [21]. Expanding on previous research, this study examines the pyrolysis kinetics of Grade 10 low-rank Indian coal under isothermal conditions, covering a temperature range of 350–500 °C in 50 °C increments at a heating rate of 20 °C/min. In addition to kinetic analysis, batch pyrolysis experiments were conducted to characterize the chemical composition of condensable pyrolytic products. The key contribution of this work lies in its comprehensive assessment of both kinetic and thermodynamic parameters during the isothermal decomposition of low-rank coal, coupled with detailed pyrolysis oil product analysis.

2 Material and methods

2.1 Coal sample

The grade 10 low-rank Indian coal sample [8] for this work is collected from the Mahanadi Coal Fields Ltd., Sambalpur, Odisha. The coal sample is ground by the householder grinder and filtered to a grid size of 100 meshes (0.149 mm). Then the required-sized coal is dehydrated by heating for 48 h at 40 °C in the air.

2.2 Characterizations of coal

Coal sample characterization was conducted following ASTM standards: moisture (ASTM D4442), volatile matter (ASTM D3172), ash (ASTM D3175), and fixed carbon (ASTM D3177). Ultimate analysis (CHNS/O content) was performed using a Vario El III CHNS analyzer (Germany) with flash combustion at 1200°C, helium carrier gas, and thermal conductivity detection. Calorific value was determined via bomb calorimetry (ASTM D5865-12). Non-isothermal pyrolysis (30–900°C, 20°C/min, 20 mL/min N_2) and isothermal pyrolysis (375–500°C, 2 h hold, 20 mL/min N_2) were conducted in a Pyris STA 8000 TGA. Samples (~9.5 mg) were heated to target temperatures at 40°C/min for isothermal tests. All experiments were triplicated to ensure reproducibility.

2.3 Batch pyrolysis study and product analysis

The batch reactor utilized in this experiment is reported in our previous experiment [20], made of a stainless steel tube with an outlet tube at one end to collect the cracked products. The pyrolysis reactor consisted of a stainless steel tube with 145 mm length and 37 mm internal diameter (41 mm external diameter). Heating was provided by an external electric furnace with temperature regulation achieved through a Shimaden PID controller (±3.6°C accuracy). Real-time temperature monitoring was performed using a K-type Cr-Al thermocouple installed inside the reactor chamber. The pyrolysis experimental temperature to yield the maximum condensable fraction is optimized by experimenting with different temperatures from 400-600 °C and found to be 450 °C [8].

For each pyrolysis trial, 30 g of coal was processed at 450°C in the reactor system. The liquid products were condensed using a 20°C water-cooled condenser and subsequently weighed, while the solid residue was measured post-pyrolysis. Gas yields were determined through mass balance calculations, with all experiments conducted in triplicate for reproducibility.

The condensed oils underwent comprehensive analysis using:

1. FTIR spectroscopy (Bruker Alpha, 500-4000 cm^{-1} range, 2 cm^{-1} resolution) with ZnSe ATR accessory for functional group identification
2. High-resolution GC-TOFMS (AccuTOF GCV, 10-2000 amu range, 6000 amu resolution) for precise compositional determination

2.4 Isothermal kinetic analysis

Isothermal kinetic analysis using model-fitting methods allows accurate determination of the kinetic triplet: reaction mechanism, activation energy, and pre-exponential (Arrhenius) factor. This research applied a model-fitting approach, incorporating four fundamental kinetic models: nucleation, geometrical contraction, diffusion, and reaction-order models. Nucleation models describe the formation and growth of new phases at imperfections in the crystal lattice, such as dislocations or impurities, and may involve complex multi-step processes. Geometrical contraction models assume that decomposition begins at the surface and progresses inward as a shrinking core, with the rate governed by the movement of the reaction front. Diffusion models, on the other hand, are based on the transport of volatile or reactive species through product layers and typically describe slower processes due to increasing diffusion resistance. Reaction-order models follow classical kinetics, where the reaction rate depends on the concentration or conversion degree raised to a defined order [22].

The rate equation for the solid-state reaction [23]:

$$\frac{d\alpha}{dt} = k\, f(\alpha)$$

$$\Rightarrow \frac{d\alpha}{f(\alpha)} = k\, dt \qquad (1)$$

We know,

$$\alpha = (m_0 - m_t)/(m_0 - m_f) \qquad (2)$$

On integrating Eq. (1)

$$\int_0^{\alpha} \frac{d\alpha}{f(\alpha)} = \int_0^{t} k\, dt$$

$$\Rightarrow g(\alpha) = k\, t + C \qquad (3)$$

The value of rate constant k at a definite temperature can be determined from the plot of $g(\alpha)$ and t based on the maximum coefficient of determination (R^2).

According to Arrhenius's equation,

$$\ln k = \ln A - \frac{Ea}{RT} \qquad (4)$$

The values of activation energy (Ea) and the pre-exponential factor (A) can be calculated using the slope and intercept from the linear graph of lnk versus 1/T. Table 1 lists the corresponding f(α) and g(α) functions [24] for various solid-state reaction mechanisms

Table 1 Value of differential and integral function of solid-state kinetic models

Model	Symbol	f(α)	g(α)
Model of Nucleation Power Law	P_2	$2\alpha^{1/2}$	$\alpha^{1/2}$
	P_3	$3\alpha^{2/3}$	$\alpha^{1/3}$
	P_4	$4\alpha^{3/4}$	$\alpha^{1/4}$
	$P_{3/2}$	$(3/2)\ \alpha^{1/3}$	$\alpha^{2/3}$
Model of Nucleation Avrami Erofeyev	A_2	$2(1-\alpha)\ [-\ln(1-\alpha)]^{1/2}$	$[-\ln(1-\alpha)]^{1/2}$
	A_3	$3(1-\alpha)\ [-\ln(1-\alpha)]^{2/3}$	$[-\ln(1-\alpha)]^{1/3}$
	A_4	$4(1-\alpha)\ [-\ln(1-\alpha)]^{3/4}$	$[-\ln(1-\alpha)]^{1/4}$
Model of Geometric Contraction	R_2	$2(1-\alpha)^{1/2}$	$1-(1-\alpha)^{1/2}$
	R_3	$3(1-\alpha)^{2/3}$	$1-(1-\alpha)^{1/3}$
Model of Diffusion	D_1	$(½)\alpha^{-1}$	α^2
	D_2	$[-\ln(1-\alpha)]^{-1}$	$(1-\alpha)\ \ln\ (1-\alpha)\ +\alpha$
	D_3	$(3/2)\ (1-\alpha)^{2/3}[1-(1-\alpha)^{1/3}]^{-1}$	$[1-(1-\alpha)^{1/3}]^2$
	D_4	$(3/2)\ [(1-\alpha)^{(-1/3)}-1]^{-1}$	$1-(2/3)\ \alpha-(1-\alpha)^{2/3}$
Model of Reaction Order	F_0	1	α
	F_1	$1-\alpha$	$[-\ln\ (1-\alpha)]$
	$F_{1.5}$	$(1-\alpha)^{3/2}$	$2[(1-\alpha)^{-1//2}-1]$
	F_2	$(1-\alpha)^2$	$[\alpha\ /(1-\alpha)]$
	$F_{2.5}$	$(1-\alpha)^{2.5}$	$(2/3)\ [(1-\alpha)^{-3/2}-1]$
	F_3	$(1-\alpha)^3$	$(1/2)\ [(1-\alpha)^{-2}-1]$
	F_4	$(1-\alpha)^4$	$(1/3)\ [(1-\alpha)^{-3}-1]$
	F_5	$(1-\alpha)^5$	$(1/4)\ [(1-\alpha)^{-4}-1]$

The pyrolysis index (I) is:

$$I=\frac{(dw/dt)_{max}}{t_{max}\Delta t} \qquad (5) \qquad [23]$$

Where, t_{max} = Time at maximum reaction rate in minute, $(dw/dt)_{max}$ = Maximum weight loss rate in percent per minute, Δt = Required amount of time in minutes for the primary reaction, and mathematically it is given:

$$\Delta t = t_f - t_i$$

Where, t_i = Time in min at $\alpha = 0.05$, t_f = Time in min at $\alpha = 0.95$

3 Result Analysis

3.1 Characterization of coal

3.1.1 Proximate, ultimate, and calorimetric analysis

From the findings of the proximate analysis, it is inferred that coal contains 24.44 % volatile chemicals, 4.16 % moisture, 44.4 % ash, and 27 % fixed carbon, respectively. The ultimate analysis reveals that it contains no nitrogen, 0.344 % sulphur, 2.38 % hydrogen, 38.81 % carbon, 58.466 % oxygen, and other metallic components. The gross calorific value of coal is 3138.01 cal/g. Coal has moisture content, which requires energy to be removed before processing. The volatile content of coal leads to the production of condensable gases, resulting in a yield of liquid and waxy products [25]. The fixed carbon content yields the production of carbonaceous products. The high ash content in coal increases handling and processing costs, decreases the rate of combustion, carbonization, and pyrolysis, and affects the efficiency of metallurgical applications [25, 26]. Therefore, during pyrolysis, a high amount of residue is

formed. The elevated carbon and hydrogen content in coal contributes to the formation of more aromatic compounds in pyrolytic products, while the higher oxygen content results in more oxygenated compounds. Coal degradation does not release NOx; however, the sulfur present (0.344%) can still contribute to the release of SOx during thermal degradation. The lower calorific value of coal is due to its higher ash, moisture, and oxygen content [25].

3.1.2 Pyrolytic degradation behavior

The thermal degradation behavior of the coal sample is studied from the thermogravimetric analysis (TGA). The thermogravimetric (TG) and derivative thermogravimetric (DTG) profiles of the coal sample are presented in Figure 1. These measurements were taken under non-isothermal conditions, using a heating rate of 20 °C/min over a temperature span from 30 to 900 °C.

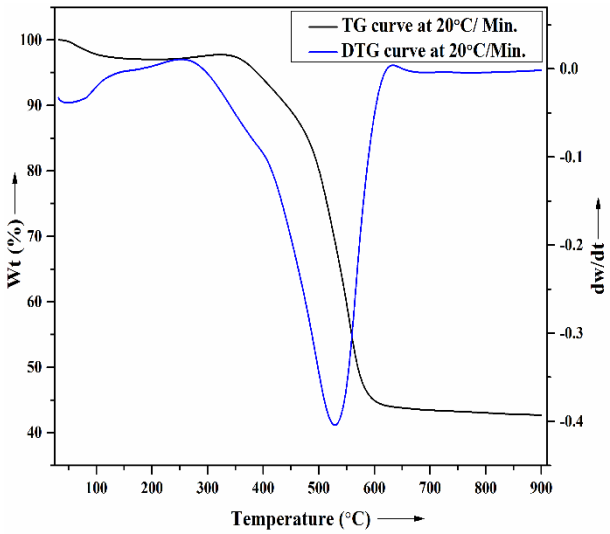

Figure 1 TG-DTG plot of the coal sample at heating rate 20ºC/min

From Fig. 1, it is clear that the pyrolysis of the coal sample in the temperature range of 30-900 °C is completed in three zones, including (i) drying of moisture and removal of volatile components (ii) degradation and devolatilization of degradation products or pyrolysis stage (iii) solid decomposition or poly-condensation heated under the non-isothermal condition. The physi-adsorbed water and highly volatile matter present in the coal are released in the first stage (30-250 °C) with a weight loss of 2.75 %. In the second zone, a prominent peak at the range of 250-630 °C in the DTG curve is found with a weight loss of 53.45 %, which is corresponds to the thermal degradation and release of volatile components and lighter frctions. In the third zone, a negligible weight of 1.05 % occurs, which corresponds to the release of CO_2 due to the degradation of carbonates in coal and the production of H_2 due to the condensation of aromatic rings in biochar [8]. Therefore, during the pyrolysis of coal under non-isothermal conditions, the total weight loss is nearly 57.25 %. The major weight loss for the coal occurs between the 250 to 630 °C temperature range. Thus, to investigate the reaction kinetics under isothermal conditions, experiments were performed at seven distinct temperatures: 350, 375, 400, 425, 450, 475, and 500 °C.

Figure 2 presents the TG-DTG curves obtained from the isothermal pyrolysis of the coal sample at constant temperatures as apecified above. The analysis reveals a two-stage pyrolytic degradation process: (1) initial non-isothermal decomposition (first peak) and (2) subsequent isothermal decomposition (second peak).

Prior to reaching the target temperature, the coal undergoes partial degradation under non-isothermal conditions. Once the desired temperature is achieved, isothermal degradation dominates. However, due to the finite heat-up period in TG analysis, true isothermal conditions are never instantaneously attained, making complete isolation of isothermal degradation

unfeasible. This inherent non-isothermal phase must be accounted for in isothermal thermogravimetric experiments [27].

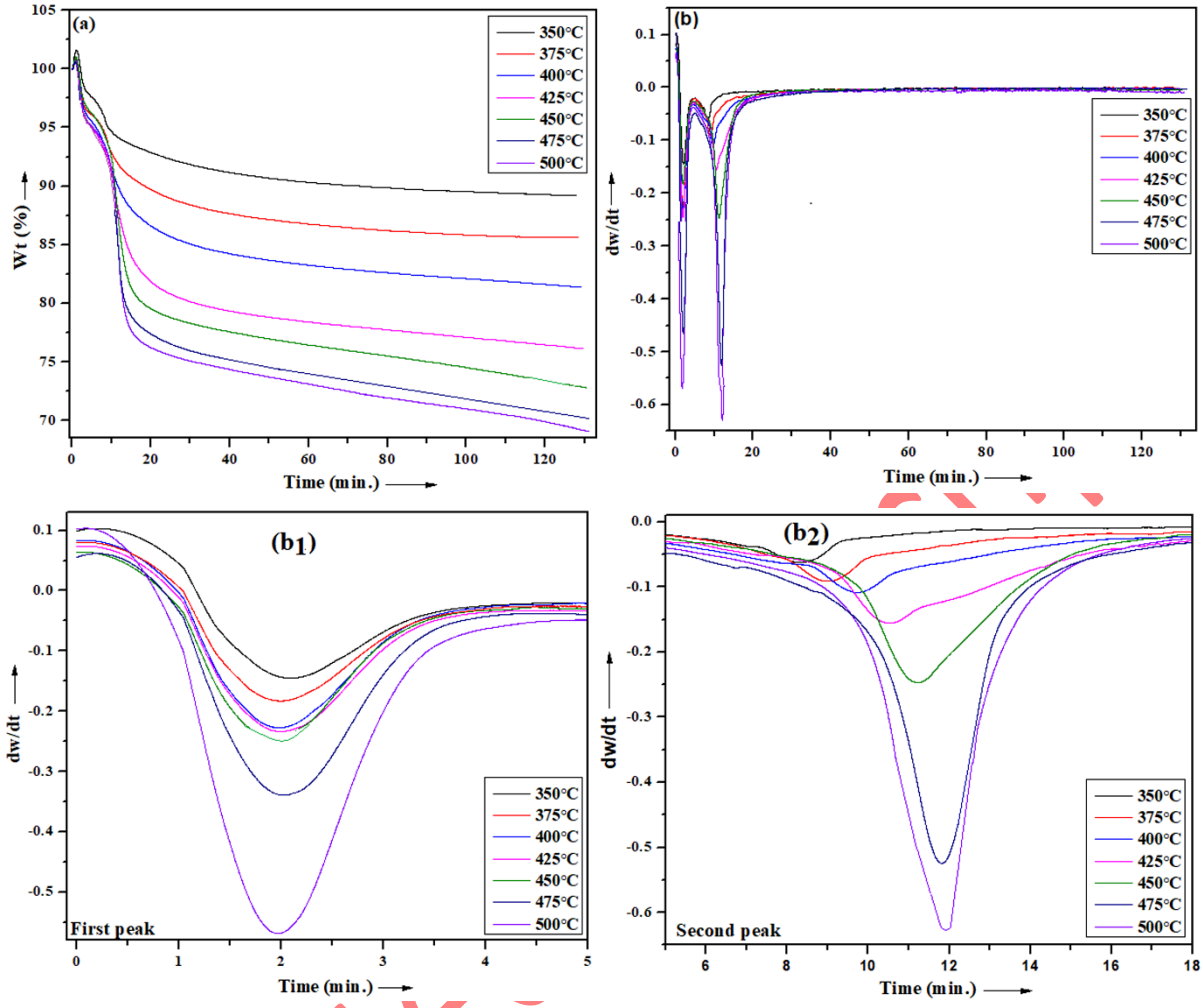

Figure 2 Isothermal (a) TG curve, (b) DTG curve, (b_1)1st peak, and (b_2) 2nd peak in DTG curve

Analysis of the thermogravimetric experimental result at different constant temperatures (Fig. 2) reveal that the onset of isothermal pyrolysis occurred at different time intervals for each temperature: 8 min (350 °C), 8.625 min (375 °C), 9.25 min (400 °C), 9.875 min (425 °C), 10.5 min (450 °C), 11.125 min (475 °C), and 11.75 min (500 °C). Table 2 summarizes the weight loss characteristics corresponding to both degradation peaks as well as the total pyrolysis process.

Table 2 Isothermal pyrolysis weight loss of coal sample

Temperature (°C)	Weight loss (%)		Total weight loss (%)
	First peak	Second peak	
350	4.000	6.832	10.832
375	5.690	8.670	14.360
400	7.422	11.196	18.618
425	8.400	15.403	23.803
450	8.680	18.610	27.290
475	13.390	16.460	29.850
500	16.355	15.605	31.960

From Table 2, two main stages of degradations can be observed, viz, (i) first Stage (Non-Isothermal): Between 350°C and 500°C, the rate of weight loss shows a consistent upward

trend with temperature. (ii) Second Stage (Isothermal): The weight loss goes up until 450°C (reaching 18.61%) but then starts decreasing at higher temperatures.
However, overall weight loss keeps increasing with temperature, with the highest loss (31.96%) occurring at 500°C. This means that while the second stage slows down after 450°C, the total decomposition still improves at higher temperatures.

.

3.2 Isothermal kinetic analysis

The isothermal degradation kinetics of coal were evaluated using multiple solid-state reaction models, as detailed in Table 1. The kinetic parameters were determined using TG data obtained under isothermal conditions. The kinetics of isothermal coal degradation are explained using different types of solid-state models, as summarized in Table 1. Plotting g(α) versus time (Eq. 3) enables calculation of the rate constant k, with the most suitable kinetic model being chosen according to the greatest coefficient of determination (R^2). Analysis of the data presented in Table 3 reveals that the D_2 diffusion model provides the most accurate representation of isothermal degradation kinetics of the coal, as evidenced by its highest regression coefficient ($R^2 = 0.940$). Fig. 3 shows the model fitting plots for diffusion models. Equivalent graphical representations can be constructed for nucleation models, geometrical contraction models, and reaction order mechanisms, with these plots serving as the basis for determining rate constants (k) in subsequent activation energy (E_a) calculations.

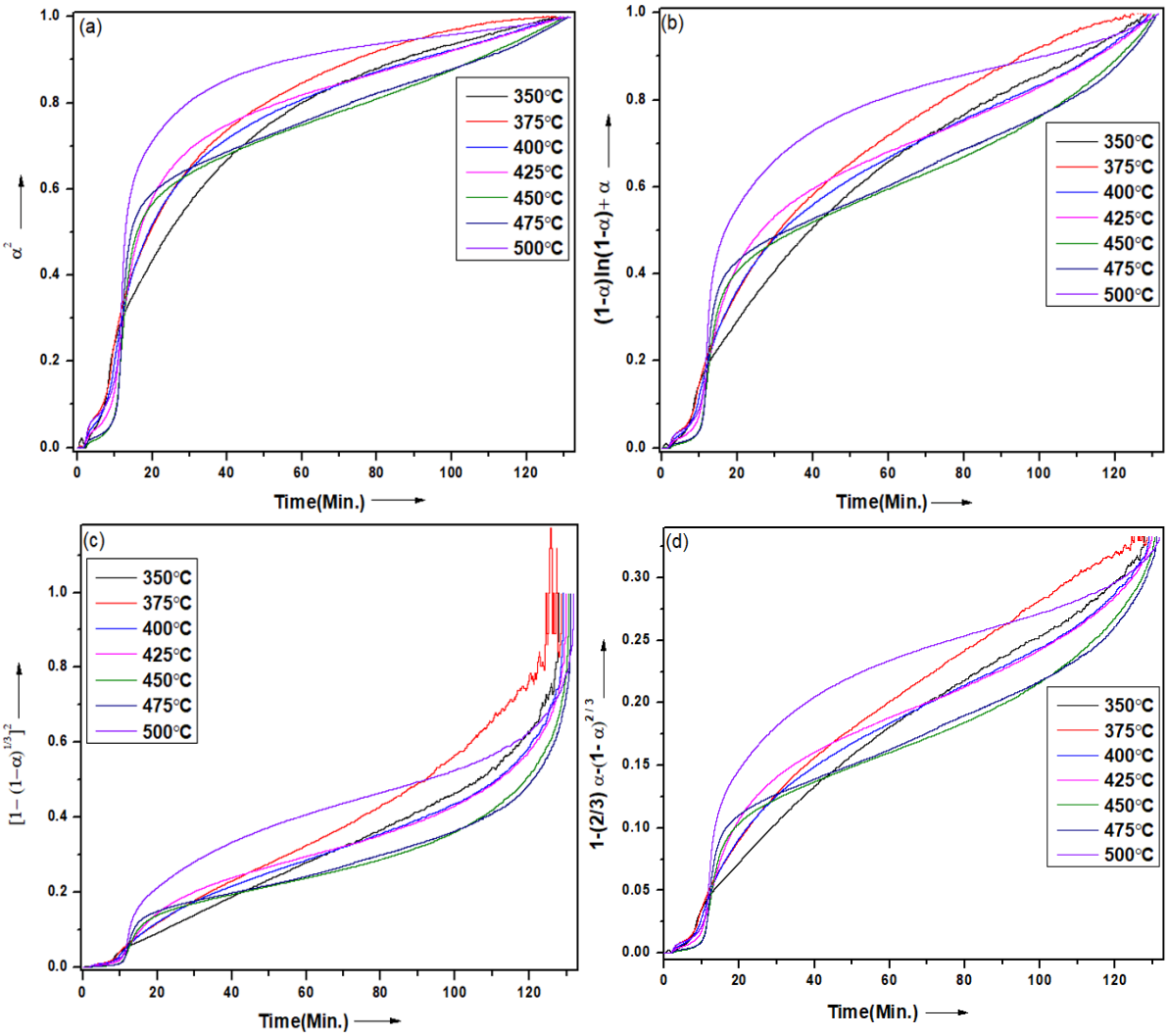

Figure 3 Model fitting plots for diffusion model [(a) D_1, (b) D_2, (c) D_3, and (d) D_4]

The derived rate constant (k) enables determination of activation energy (E_a) and pre-exponential factor (A) through Arrhenius analysis, achieved by plotting lnk against reciprocal temperature (1/T) as described in Equation 4. As illustrated in Figure 4, the temperature dependence of rate constants (ln k vs. 1/T) was analyzed for each kinetic model (nucleation, geometrical contraction, diffusion, and reaction order) , yielding the E_a and A parameters summarized in Table 3.

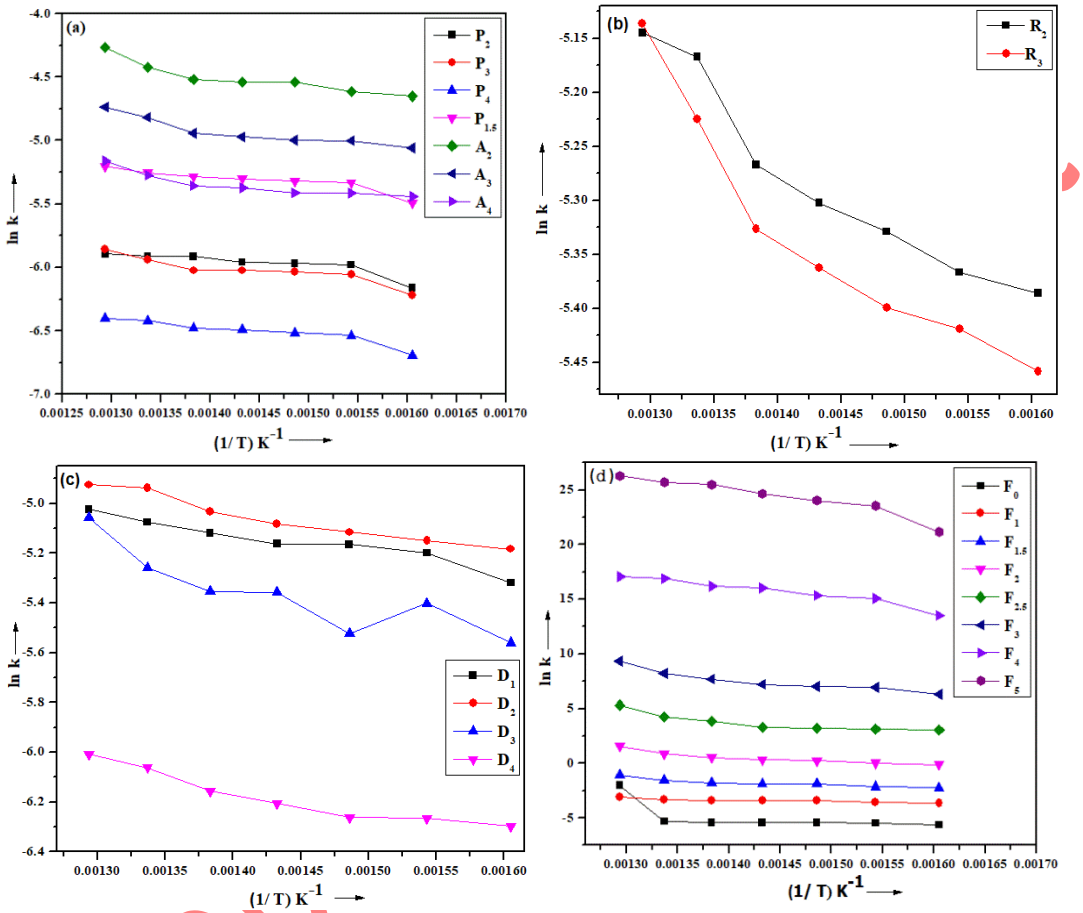

Figure 4 Linear model fitting kinetic plots for (a) nucleation model, (b) contracting area model, (c) diffusion model, and (d) reaction order model

Table 3 Kinetic parameters from different models

Reaction Model	R^2	Ea (kJ/mol)	A(min^{-1})
Nucleation Model			
P_2	0.706	5.817	0.007
P_3	0.821	7.605	0.009
P_4	0.850	6.680	0.005
$P_{1.5}$	0.014	6.164	0.806
A_2	0.810	8.794	0.051
A_3	0.812	7.791	0.028
A_4	0.770	12.760	0.300
Geometrical Contraction Model			
R_2	0.911	6.695	0.016
R_3	0.868	8.025	0.019
Diffusion Method			

D_1	0.921	6.783	0.019
D_2	0.940	7.267	0.022
D_3	0.732	11.008	0.032
D_4	0.893	7.791	0.008
Reaction Order Model			
F_0	0.270	60.191	236.633
F_1	0.857	12.759	0.300
$F_{1.5}$	0.830	26.964	17.765
F_2	0.829	39.657	1.591×10^{3}
$F_{2.5}$	0.708	53.041	4.043×10^{3}
F_3	0.857	70.221	3.582×10^{8}
F_4	0.930	87.827	2.727×10^{13}
F_5	0.907	123.516	7.738×10^{19}

Based on this optimal model, the calculated activation energy and Arrhenius frequency factor for the process are 7.267 kJ/mol and 0.022 min^{-1}, respectively. It should be noted that activation energy values obtained from alternative kinetic models show considerable variation, ranging from 5.817 to 123.51 kJ/mol.

Nucleation models are too simple. The models assume the material is uniform and conditions are ideal. In reality, materials have impurities and uneven structures. Temperature and pressure can change quickly, which is not considered in the models. Nucleation also focuses too much on thermodynamics and ignores how fast changes happen. Because of this, nucleation models do not work well for complex processes like coal pyrolysis. The Geometrical Contraction Model fails because it oversimplifies reaction dynamics, especially in complex systems like coal pyrolysis, where the material undergoes significant structural changes. The model assumes uniform shrinking of the unreacted core and a predictable inward-moving reaction front. In reality, reactions involve porous structure formation, changing surface areas, and diffusion limits, which the model ignores. In coal pyrolysis, gas and liquid products can create internal pressure, altering porosity and causing uneven shrinkage. The model also assumes a constant reaction rate, while real systems experience variable rates due to temperature gradients, concentration changes, and material heterogeneity. These factors make the model unreliable for non-uniform or dynamic processes. The Reaction Order Model often fails because it oversimplifies complex chemical processes, especially when reaction mechanisms are unclear or involve multiple steps. It assumes the reaction rate depends solely on reactant concentrations raised to a fixed power, which is inaccurate in systems where pathways change over time or under varying conditions. In processes like coal pyrolysis, intermediate steps like diffusion or chemical rearrangements are not captured by a simple rate equation. The model also assumes constant activation energy and a uniform mechanism, which do not hold in heterogeneous systems with temperature gradients or varying material properties. This leads to significant differences between predicted and actual behavior. The diffusion method is often successful because it accurately reflects how reactions are controlled by the movement of reactants or products, especially in systems with porous materials, like coal. In processes like coal pyrolysis, the chemical reaction might happen quickly, but the rate at which gases or reactants can move through the material often limits the overall reaction rate. Diffusion models take this into account, explaining why reactions slow down as time passes. These models also match better with experimental observations, especially when the activation energy is lower, indicating that diffusion, rather than chemical reactions, is the limiting step [28].

The high ash content in coal reduces its energy density, as ash is inert and does not contribute to pyrolysis. It also impedes heat and mass transfer, which can increase the activation energy required for thermal degradation. Despite this, the relatively low activation energy calculated

in this study may be attributed to the high volatile matter and fixed carbon contents, which enhance reactivity. Volatile matter facilitates the release of fuel gases and accelerates reaction rates, while fixed carbon supports sustained combustion [25]. Moreover, the low activation energy aligns with a diffusion-controlled mechanism, as diffusion processes typically require less energy than chemical reaction-limited steps, supporting the applicability of the D_2 diffusion model to coal pyrolysis [28]. Table 4 presents the kinetic results for various low-rank coals under different experimental conditions.

Table 4 Kinetic Results of Different Low-Rank Coals

Low rank Coal	**Kinetic Method**	**Experimental condition**	**Ea (kJ/mol)**	**A (min^{-1})**	**Ref.**
Grade-10	Model-fitting	Temperature = 375, 400, 425, 450, 475, and 500 °C, Heating rate = 40 °C/min, Reaction time = 2 h, and Nitrogen flow rate = 20 mL/min	7.267	0.022	Current Study
Grade-10 Grade-13 Grade-14	Coats Redfern	Temperature range = 30–1000 °C, Heating rate = 5, 10, 15, 20, and 25 °C/min, and Nitrogen flow rate = 40 mL/min	62.114 61.940 57.563	5.190×10^{5} 3.655×10^{5} 4.257×10^{4}	Previous study [8]
Indian low-grade coal	Friedman	Temperature range = 30–950 °C, Heating rate = 50, 100, 150, and 200 K/min, Nitrogen flow rate = 40 mL/min	49.132	188.88	[6]
Chinese Western low-rank coal	Pseudo-first order	Temperature range = 25-500 °C, Heating rate = 10, 20, and 30 °C/min, and Nitrogen flow rate = 100 mL/min	113.170	7.975×10^{9}	[15]
Indian high-ash coal	Friedman	Temperature range = Room temperature to 1173 K, Heating rate = 278, 293, 323, 373, 573, 773 K/min, and Nitrogen flow rate = 60 mL/min	428.78-520	2.920×10^{36}	[9]
Shenhua coal	Coats–Redfern	Temperature range = Room temperature to 900 °C, Heating rate = 10, 15, and 20 °C/min, and Nitrogen flow rate = 40 mL/min	140.44	1.737×10^{15}	[13]
Lignite NCC LFC (Heilongjiang) LFC (Shandong)	Distributed Activation Energy Model	Temperature range = Room temperature to 1050 °C, Heating rate = 5, 10, 20, and 30 °C/min, and Nitrogen flow rate = 50 mL/min	331 298 302 196	----- ----- ----- -----	[29]
Lignite			37.97	240.20	[30]

NCC LFC (Heilongjiang) LFC (Shandong)	Doyle's integral method	Temperature range = Room temperature to 1050 °C, Heating rate = 10 °C/min, and Nitrogen flow rate = 50 mL/min	40.40 48.59 42.4	195.62 4645.45 1204.27	
Lignite and subbituminous coal	Kissinger, KAS, FWO, Friedman	Temperatures range = 298-1173 K, Heating rate = 1, 6, 9, 12, 15, and 18 K/min, and Nitrogen flow rate = 100mL/min	281, 282, 275, 283	2.61×10^{17}, 2×10^{20}, 1.07×10^{27}, 1.89×10^{23}	[31]

3.3 Pyrolysis Index

The pyrolysis index is influenced by the maximum pyrolysis rate and reaction time. In terms of reaction rate, a higher pyrolysis index indicates better pyrolysis performance [23]. The pyrolysis index for coal at different temperatures is calculated using Eq. (5) and listed in Table 5.

Table 5 Pyrolysis index

T (°C)	t_i (min)	t_{max} (min)	t_f (min)	DTG_{max} (% min^{-1})	I (% min^{-3})
First Peak					
350	2.20	2.10	4.62	14.38	2.830
375	1.80	2.09	4.44	18.24	3.306
400	1.72	2.05	4.43	22.67	4.081
425	1.66	2.03	4.38	23.29	4.218
450	1.54	1.99	4.28	24.98	4.582
475	1.53	1.98	4.25	33.87	6.289
500	1.49	1.97	4.15	56.80	10.839
Second Peak					
350	6.12	8.35	72.96	6.30	0.011
375	6.44	9.01	83.26	9.02	0.013
400	6.57	9.72	85.31	10.81	0.014
425	6.92	10.55	100.59	15.46	0.016
450	7.04	11.24	101.45	24.67	0.023
475	7.32	11.59	110.37	52.36	0.044
500	7.69	11.92	112.71	62.87	0.051

As a result of the DTG curve having two peaks, the pyrolysis index for the sample cannot be precisely calculated. The first peak corresponds to non-isothermal degradation, but the second peak corresponds to isothermal degradation. Therefore, the pyrolysis index variation in the first peak concerning time parameters (t_i, t_{max}, and t_f) is contradictory to that in the second peak. The pyrolysis index for first-stage degradation increases with increases in temperature from 350 °C to 500 °C. However, for this work, the second stage of degradation plays an important role, which also increases from 350 °C to 500 °C. According to Table 5, the second step of the pyrolytic degradation of coal results in much better pyrolysis performance at 500 °C than at other temperatures.

3.4 Batch pyrolysis results

From the isothermal kinetic analysis, it is found that the maximum degradation is observed at 450 °C. Thus, the batch pyrolysis experiment is carried out at this temperature to obtain the condensable fraction. Different products, viz. the condensable fraction (18.9 %), the non-condensable fraction (1.9 %), and the residue (79.2 %), are formed during the experiment. The

condensable fraction is a dark black coloured liquid. The high ash content in coal leads to the formation of a large amount of residue during thermal processing [25]. The reaction time for the batch pyrolysis of low rank coal is 95 minutes. Fig. 5 illustrates the relationship between the pyrolytic fraction and the yield.

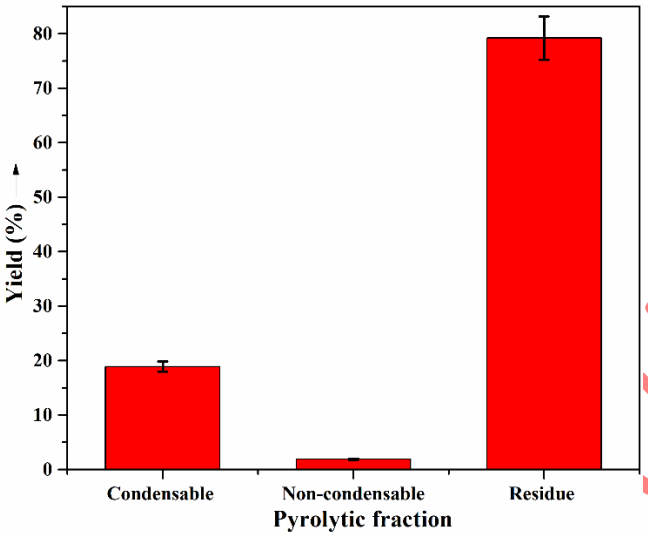

Figure 5 Plot of pyrolytic product distribution

3.4.1 Composition of pyrolytic oil using GC-MS and FTIR

The composition of the liquid fraction is confirmed using GC-MS and FTIR analysis. The Gas chromatography-mass spectrometry plot for the oil formed at 450 °C during pyrolysis of coal under isothermal conditions is represented in Fig. 6.

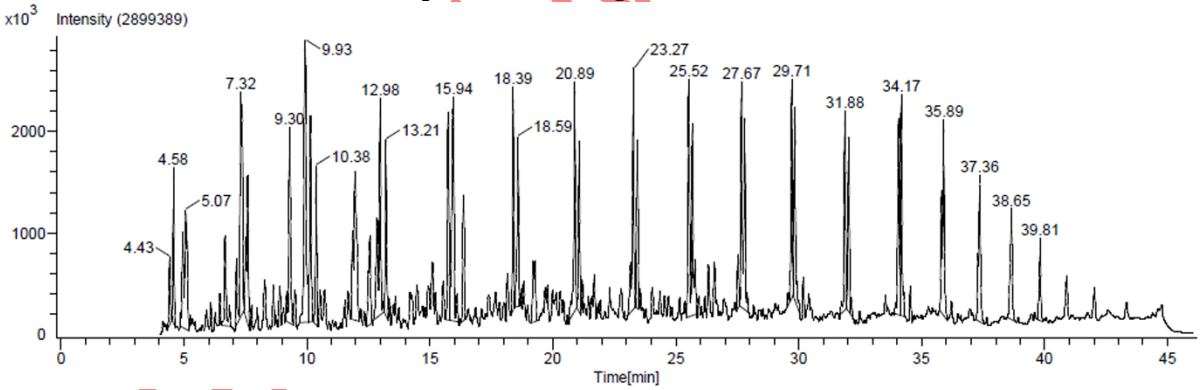

Figure 6 GC-MS plot of the coal pyrolytic oil @ 450 °C

Table 6 contains a list of compounds in the pyrolytic oil as analysed using GC-MS. Three different categories of compounds, such as aliphatic alkane, alicyclic, and aromatic compounds, are identified in the oil. The aliphatic alkanes constitute 16.48 % of pyrolytic oil with C_{15}-C_{21}. Heptadecane has the largest area percentage among all aliphatic alkanes at 11.23 %, in addition to pentadecane and octadecane. The oil contains 35.25 % alicyclic compounds with C_{12}-C_{15}, with D-Limonene (28.45 %) having the highest area percentage in alicyclic compounds. The third and highest fraction among the three categories is aromatic compounds (48.27 %) with C_6-C_{20}. The majority of the components in this category include phenol and its derivatives, with 4-methylphenol (12.05 %) having the highest area percentage.

Table 6 GC-MS component analysis of coal pyrolytic oil

Compound	**Molecular Formula**	**Area %**

(1) Aliphatic alkane		**16.48**
Heptadecane	$C_{17}H_{36}$	11.23
Pentadecane	$C_{15}H_{32}$	2.20
Octadecane	$C_{18}H_{38}$	1.70
2,6,10,15-tetramethyl heptadecane	$C_{21}H_{44}$	1.35
(2) Alicyclic Compound		**35.25**
D-Limonene	$C_{10}H_{16}$	28.45
3,7,7-trimethyl-11-methylene spiro [5.5] undec-2-ene	$C_{15}H_{24}$	3.74
7,7-dimethyl bicyclo [3.1.1] hept-3-ene-spiro-2,4-(1,3-dioxane)	$C_{12}H_{18}O_2$	3.06
(3) Aromatic compound		**48.27**
4-methyl phenol	C_7H_8O	12.05
Phenol	C_6H_6O	8.17
2,4-dimethyl phenol	$C_8H_{10}O$	7.75
2-methyl phenol	C_7H_8O	6.25
o-[(1,2,3,4-tetrahydro-2-naphthyl) methyl] hydro cinnamic acid	$C_{20}H_{22}O_2$	5.82
1,1(1,3-propanediyl) bisbenzene	$C_{15}H_{16}$	3.88
1-ethyl-2,3-dihydro-1-methyl-1H-Indene	$C_{12}H_{16}$	2.47
1-ethylidene-1H-Indene	$C_{11}H_{10}$	1.88

The FTIR spectrum of the oil obtained from coal pyrolysis at 450 °C is presented in Fig. 7. Key absorption peaks are observed at 1726 cm^{-1} (C=O stretching), 1216 cm^{-1} (C-O stretching), and 720 cm^{-1} (O-H out-of-plane bending), which are characteristic of carboxylic acid functional groups. These findings align with the identification of o-[(1,2,3,4-tetrahydro-2-naphthyl)methyl]hydrocinnamic acid in Table 6, confirming its presence in the pyrolytic oil. The FTIR spectrum also exhibits characteristic peaks at 2920 cm^{-1} (asymmetric C-H stretching of methylene groups), 2850 cm^{-1} (symmetric C-H stretching of methylene groups), 909 cm^{-1} (C=C stretching), 1473 cm^{-1} (asymmetric CH_3 bending), and 1376 cm^{-1} (symmetric CH_3 bending). These absorption bands indicate the presence of long-chain aliphatic hydrocarbons in the pyrolytic oil, which is further corroborated by GC-MS analysis. The FTIR spectrum displays characteristic peaks at 1603 cm^{-1}, attributed to C=C skeletal vibrations and aromatic ring stretching, and at 1376 cm^{-1}, associated with in-plane bending vibrations. These absorption bands indicate the presence of phenolic compounds in the pyrolytic oil. Additionally, the peak observed at 720 cm^{-1}, corresponding to out-of-plane bending, further supports the existence of phenol derivatives such as 4-methyl phenol, 2,4-dimethyl phenol, and 2-methyl phenol. These findings are consistent with the compound identification obtained through GC-MS analysis. The absorption band at 909 cm^{-1} can be attributed to out-of-plane bending vibrations, potentially indicating the presence of alicyclic structures. This spectral feature suggests compounds such as D-limonene, 3,7,7-trimethyl-11-methylene-spiro[5.5]undec-2-ene, and 7,7-dimethylbicyclo[3.1.1]hept-3-ene-spiro-2,4-(1,3-dioxane) may be present in the sample [32].

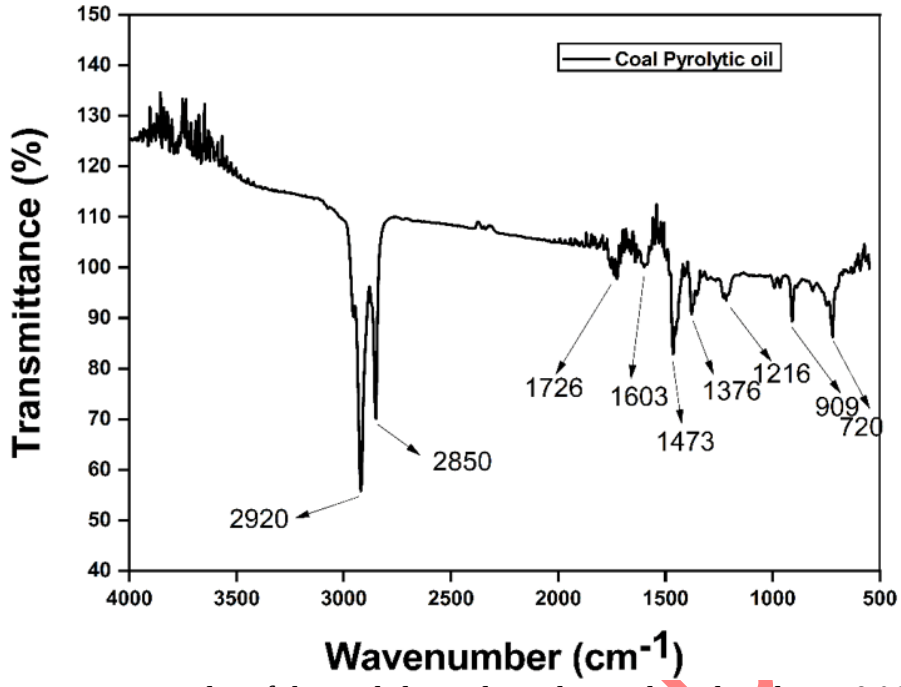

Figure 7 FTIR plot of the coal-derived pyrolytic oil produced at 450 °C

4 Conclusion

The pyrolytic degradation behaviors and kinetics of coal under isothermal conditions are studied using the TGA technique. Model-fitting kinetic equations concerning different mechanisms are used to compute the kinetic parameters. There is a noticeable increase in overall weight loss in isothermal conditions with rising temperatures. The maximum % weight loss under isothermal conditions is 18.61 % at 450 °C. The activation energy for the reaction ranges between 5.817 and 123.51 kJ/mol, depending on the model used. Under isothermal conditions, coal pyrolysis degradation best fits the D2 diffusion model, yielding an activation energy (Ea) of 7.267 kJ/mol and a pre-exponential factor (A) of 0.022 min^{-1}, based on the highest regression coefficient (R^2) criterion. Aliphatic alkanes, including heptadecane, pentadecane, octadecane, and heptadecane, are detected in addition to alicyclic and aromatic compounds in the pyrolytic oil produced by the isothermal pyrolysis of coal at 450 °C. Using effective methods, the pyrolytic mixture products may be separated into usable compounds.

Nomenclature

(i) Roman Symbols

Roman Symbol	**Definition**	**Unit**
A	Arrhenius constant	$minute^{-1}$
C	Integration constant	----
Ea	Activation energy	kJ/mol
I	Pyrolysis index	% min^{-3}
K	Rate constant	$minute^{-1}$
M	Mass	mg
R	Gas constant	$kJmol^{-1}K^{-1}$
R^2	Coefficient of determination	----
t	Reaction time	minute
T	Temperatures	°C, and K
W	Weight	mg, and g
f(α)	Function of differential reaction mechanism	----

$g(\alpha) = \int_0^{\alpha} \frac{d\alpha}{f(\alpha)}$	Integral form of the mechanism	-----
$\frac{d\alpha}{dt}$	Rate of Reaction	Moles $l^{-1}s^{-1}$
m_0	Initial mass	g
m_t	Instantaneous mass at a certain time t	g
m_f	Final mass	g

(ii) Greek Letters

Greek Letter	Definition	Unit
α	Degree of Conversion	----

Abbreviation

ASTM	American Society for Testing and Materials
ATR	Attenuated Total Reflectance
CC	Chamalang Coal
CHNS	Carbon, Hydrogen, Nitrogen, Sulphur
CI	Chemical Ionization
DC	Dukki Coal
DLATGA	Deuterated L-alanine doped triglycene sulphate
DTG	Differential Thermogravimetry
EI	Electron Ionization
FTIR	Fourier Transform Infrared
FWO	Flynn-Wall-Ozawa
GC-MS	Gas chromatography-mass spectrometry
GCV	Gas Chromatography-Vacuum
HCC	Hard coking coal
KAS	Kissinger-Akahira-Sunose
LFC	Long-flame coal
MCL	Mahanadi Coalfields Limited
MS	Mass Spectrometer
NCC	Non-caking coal
OPUS	Online Publikationsverbund der Universitat Stuttgart
PID	Proportional – Integral – Derivative
STA	Simultaneous Thermal Analyzer
TGA	Thermogravimetry analysis
TOF	Time-of-flight
WCC	Weak coking coal

Reference

[1] Balat M. Coal in the global energy scene. Energy Sources, Part B: Economics, Planning, and Policy. 2009 Dec 28;5(1):50-62. https://doi.org/10.1080/15567240701758927.

[2] Provisional coal statistics 2022-23, Ministry of coal, Government of India. https://coal.nic.in/sites/default/files/2023-10/17-10-2023a-wn.pdf, Date of acess: 29th April 2025

[3] Qaisar SH, Ahmad MA. Production, consumption and future challenges of coal in India. International Journal of Current Engineering and Technology. 2014;4(5):3437-40. https://citeseerx.ist.psu.edu/document?repid=rep1&type=pdf&doi=529d147a661b3de112c2a931582737f953b33440.

[4] Coal in India. https://en.wikipedia.org/wiki/Coal_in_India, Date of acess :3rd October 2022

[5] Ramkumar M, Santosh M, Mathew MJ, Siddiqui NA. India at crossroads for energy. Geoscience Frontiers. 2021 Nov 1;12(6):100901.https://doi.org/10.1016/j.gsf.2019.10.006.

[6] Dwivedi KK, Chatterjee PK, Karmakar MK, Pramanick AK. Pyrolysis characteristics and kinetics of Indian low rank coal using thermogravimetric analysis. International Journal of Coal Science & Technology. 2019 Mar;6:102-12. https://doi.org/10.1007/s40789-019-0236-7.
[7] Unlocking Transparency by Third Party Assessment of Mined Coal, UTTAM, Ministry of Coal, Government of India, https://uttam.coalindia.in/about.html#:~:text=Lignite:%20It%20is%20the%20lowest,Nadu%2C%20and%20Jammu%20&%20Kashmir, Date of access: 29th April 2025
[8] Sabat G, Gouda N, Panda AK. Effect of coal grade and heating rate on the thermal degradation behavior, kinetics, and thermodynamics of pyrolysis of low-rank coal. International Journal of Coal Preparation and Utilization. 2023 Jun 3;43(6):1057-75. https://doi.org/10.1080/19392699.2022.2096013.
[9] Dong L, Vuthaluru H, French D, Karmakar S, Sutrakar AK, Satyakam R. Indian coal pyrolysis behaviour and kinetics study using covalent bond information. Thermochimica Acta. 2022 May 1;711:179208. https://doi.org/10.1016/j.tca.2022.179208.
[10] Prabhakar A, Sadhukhan AK, Gupta P. Study of pyrolysis kinetics of coal fines using model free method. Materials Today: Proceedings. 2022 Jan 1;68:910-5. https://doi.org/10.1016/j.matpr.2022.07.079.
[11] Yan J, Liu M, Feng Z, Bai Z, Shui H, Li Z, Lei Z, Wang Z, Ren S, Kang S, Yan H. Study on the pyrolysis kinetics of low-medium rank coals with distributed activation energy model. Fuel. 2020 Feb 1;261:116359.https://doi.org/10.1016/j.fuel.2019.116359.
[12] Casal MD, Vega MF, Diaz-Faes E, Barriocanal C. The influence of chemical structure on the kinetics of coal pyrolysis. International Journal of Coal Geology. 2018 Jul 1;195:415-22. https://doi.org/10.1016/j.coal.2018.06.014.
[13] Guo Z, Zhang L, Wang P, Liu H, Jia J, Fu X, Li S, Wang X, Li Z, Shu X. Study on kinetics of coal pyrolysis at different heating rates to produce hydrogen. Fuel processing technology. 2013 Mar 1;107:23-6.https://doi.org/10.1016/j.fuproc.2012.08.021.
[14] Ashraf A, Sattar H, Munir S. Thermal decomposition study and pyrolysis kinetics of coal and agricultural residues under non-isothermal conditions. Fuel. 2019 Jan 1;235:504-14. https://doi.org/10.1016/j.fuel.2018.07.120.
[15] Gao Z, Zheng M, Zhang D, Zhang W. Low-temperature pyrolysis properties and kinetics of non-coking coal in Chinese western coals. Journal of the Energy Institute. 2016 Nov 1;89(4):544-59. https://doi.org/10.1016/j.joei.2015.07.002.
[16]Vyazovkin S, Wight CA. Isothermal and non-isothermal kinetics of thermally stimulated reactions of solids. International reviews in physical chemistry. 1998 Jul 1;17(3):407-33.https://doi.org/10.1080/014423598230108.
[17] Jeong HM, Seo MW, Jeong SM, Na BK, Yoon SJ, Lee JG, Lee WJ. Pyrolysis kinetics of coking coal mixed with biomass under non-isothermal and isothermal conditions. Bioresource technology. 2014 Mar 1;155:442-5.https://doi.org/10.1016/j.biortech.2014.01.005.
[18] Zhang Y, Zhao M, Linghu R, Wang C, Zhang S. Comparative kinetics of coal and oil shale pyrolysis in a micro fluidized bed reaction analyzer. Carbon Resources Conversion. 2019 Dec 1;2(3):217-24.https://doi.org/10.1016/j.crcon.2019.10.001.
[19] Lazaro MJ, Moliner R, Suelves I. Non-isothermal versus isothermal technique to evaluate kinetic parameters of coal pyrolysis. Journal of Analytical and Applied Pyrolysis. 1998 Oct 1;47(2):111-25.https://doi.org/10.1016/S0165-2370(98)00083-7.
[20] Sabat G, Gouda N, Panda AK. Pyrolysis of low- rank coal: Thermo- kinetic analysis and product characterization. Environmental Quality Management. 2022 Dec;32(2):73-83. https://doi.org/10.1002/tqem.21911.
[21] Vyazovkin S, Chrissafis K, Di Lorenzo ML, Koga N, Pijolat M, Roduit B, Sbirrazzuoli N, Sunol JJ. ICTAC Kinetics Committee recommendations for collecting experimental thermal

analysis data for kinetic computations. Thermochimica Acta. 2014;590:1–23. https://doi.org/10.1016/j.tca.2014.05.036.
[22] Mahapatra PM, Gouda N, Pradhan D, Mishra PC, Mishra P, Panda AK. Isothermal co-pyrolytic kinetics investigation of polystyrene/polymethyl methacrylate blended Bakelite. Canadian Journal of Chemical Engineering. https://doi.org/10.1002/cjce.25505.
[23] Hu DH, Chen MQ, Huang YW, Wei SH, Zhong XB. Evaluation on isothermal pyrolysis characteristics of typical technical solid wastes. Thermochimica Acta. 2020 Jun 1;688:178604. https://doi.org/10.1016/j.tca.2020.178604.
[24] Sahoo A, Kumar S, Mohanty K. Kinetic and thermodynamic analysis of Putranjiva roxburghii (putranjiva) and Cassia fistula (amaltas) non-edible oilseeds using the thermogravimetric analyzer. Renewable Energy. 2021 Mar 1;165:261-277.https://doi.org/10.1016/j.renene.2020.11.011.
[25] Mahapatra PM, Kumar S, Mishra P, Panda AK. Effect of different thermoplastics on the thermal degradation behavior, kinetics, and thermodynamics of discarded bakelite. Environmental Science and Pollution Research. 2024;31(27):38788–38800. https://doi.org/10.1007/s11356-023-25953-2.
[26]Sharma S, Ghoshal AK. Study of kinetics of co-pyrolysis of coal and waste LDPE blends under argon atmosphere. Fuel. 2010;89:3943–3951. https://doi.org/10.1016/j.fuel.2010.06.033
[27] Vyazovkin S, Burnham AK, Criado JM, Pérez-Maqueda LA, Popescu C, Sbirrazzuoli N. ICTAC Kinetics Committee recommendations for performing kinetic computations on thermal analysis data. Thermochimica Acta. 2011 Jun 10;520(1-2):1-9. https://doi.org/10.1016/j.tca.2011.03.034.
[28] Ammar Khawam and Douglas R. Flanagan, The Journal of Physical Chemistry B 2006 110 (35), 17315-17328, https://doi.org/10.1021/jp062746a.
[29] Song H, Liu G, Wu J. Pyrolysis characteristics and kinetics of low-rank coals by distributed activation energy model. Energy Conversion and Management. 2016;126:1037–1046. https://doi.org/10.1016/j.enconman.2016.08.082.
[30] Song H, Liu G, Zhang J, Wu J. Pyrolysis characteristics and kinetics of low-rank coals by TG-FTIR method. Fuel Processing Technology. 2017;156:454–460. https://doi.org/10.1016/j.fuproc.2016.10.008
[31] Heydari M, Rahman M, Gupta R. Kinetic study and thermal decomposition behavior of lignite coal. International Journal of Chemical Engineering. 2015;2015:Article ID 481739, 9. https://doi.org/10.1155/2015/481739.
[32] Sharma, Y. R. Elementary organic spectroscopy. S. Chand Publishing. 2007

Acknowledgments
We sincerely acknowledge TEQIP-III, VSSUT, Burla, for providing the instrumental facilities necessary to characterize the samples in this research.

Data Availability:
The corresponding author may be requested for the data availability.

Declarations

Ethical Approval
Not applicable.

Consent to Participate
All the authors gave consent to participate.

Consent for Publication
All the authors gave explicit consent to submit the work to the Journal of Chemical and Petroleum Engineering.

Funding
The authors declare that no funds, grants, or other support were received during this work.

Competing Interests

The authors have no relevant financial or non-financial interests to disclose.